

Decay of a Passive Scalar in Stretched Grid Turbulence

S. K. Lee, L. Djenidi and R. A. Antonia

School of Engineering, The University of Newcastle, N.S.W., 2308 AUSTRALIA

Abstract

Approximately homogeneous isotropic turbulence (HIT) is produced by passing a uniform flow through a grid followed by a 1.36:1 contraction. The contraction stretches the flow in the streamwise direction and so reduces the anisotropy of the grid turbulence. This paper presents measurements of a passive scalar in HIT, and so extends the work of Lavoie [6] and Benaissa et al. [3]. A wind-tunnel grid flow is slightly heated ($\Delta T \approx 2^\circ\text{C}$) by a second fine-wire grid so that temperature acts as a weak scalar contaminant. For three different grids, the variance of the scalar fluctuation ($\theta'^2/\Delta T^2$) is measured over the full length of the test section. The amplitude of temperature fluctuation is well represented by the power-law decay $\theta'^2/\Delta T^2 = \alpha[(t-t_0)U_0/M]^n$. With least-square curves of best fit, the r.m.s. difference between the power law and the data is no more than 1%. All numerical coefficients (t_0 , α and n) depend on the geometry of the grid (or the initial/boundary conditions of the flow). In comparison with the square-grid data of Zhou et al. [12], these results show that the effect of the contraction is to increase the decay exponent from -1.46 to -1.18 .

Introduction

The purpose of the research reported here is to improve our understanding of turbulent mixing. Measurements of a passive scalar are obtained in approximately homogeneous isotropic turbulence. The passive scalar is a property of the fluid which has no effect on the dynamics of the flow; in this case the passive scalar is temperature. Homogeneous isotropic turbulence (HIT¹) is the least complex form of turbulence and is approximated experimentally in the decaying velocity and temperature fluctuations downstream of a grid. The turbulence in this flow decays because there is no mean shear and hence no production of turbulence kinetic energy. The study of scalar fluctuations is of interest because the mixing of scalar quantities is at the core of phenomena such as dispersion of pollutants and combustion.

In the flow under consideration, turbulence is produced by three different biplanar grids of uniformly spaced square or round bars, as shown in Figure 1. The vertical and horizontal bars in the grid are in contact. By measuring $1.2 < u'^2/w'^2 < 1.5$ for the ratio of streamwise to cross-stream velocity fluctuations, Lavoie [6] shows that the grid turbulence is anisotropic. To reduce the anisotropy, he [6] inserts a contraction downstream of the grid and finds that, with a contraction area ratio of 1.36, the turbulence is less anisotropic ($0.9 < u'^2/w'^2 < 1.2$). The contraction changes the anisotropy by stretching the flow. In particular, for round bars wrapped with a helix of wire to reduce periodic shedding, Lavoie [6] finds that using this grid (known as "Rd44w") with the contraction produces a nearly isotropic turbulence ($u'^2/w'^2 \approx 0.99$).

Reducing the anisotropy of an experimental flow allows more accurate testing of developments in the theory of turbulence.

¹In HIT, the free-stream velocity is uniform and the variance of streamwise fluctuation $u(x)^2$ is equal to the variance of cross-stream fluctuations $v(y)^2$, $w(z)^2$ (the dash denotes the r.m.s.; e.g. $u' = \sqrt{u^2}$). All three components of fluctuating signal have a normal distribution.

Many studies of grid turbulence [2, 5, 9, 11] suggest that the decay of velocity variance ($q'^2 = u'^2 + v'^2 + w'^2$) and of scalar variance (θ'^2) follow power laws ($q'^2 \propto x^m$, $\theta'^2 \propto x^n$), where the decay exponents ($m, n < 0$) depend on grid geometry and Reynolds number.

Before the present work, the only available temperature data which compares the different grids studied by Lavoie [6] was from Benaissa et al. [3]. In their [3] experiments, the decay exponents (n) are obtained from measurements in the region $25 \lesssim x/M \lesssim 77$. The current paper extends the region of measurements in stretched grid turbulence to $18 \lesssim x/M \lesssim 100$ and it includes measurements of skewness and kurtosis of temperature fluctuations.

Apparatus

Figure 1 shows the three grids which match those reported by Benaissa et al. [3], one of square bars at 35% solidity (Sq35) and two of round bars at 35% and 44% solidity (Rd35, Rd44w). The mesh pitch for each grid is $M = 24.76$ mm. The results are obtained using the same wind tunnel as that used by Lavoie [6] and Benaissa et al. [3], and the tests are run at the same mesh Reynolds number $Re_M = MU_0/\nu = 10,400$. Taylor micro-scale λ is in the range ($25 < \lambda u'/\nu < 55$).

Comte-Bellot and Corrsin [4] have discussed the method of reducing the anisotropy of grid turbulence with a contraction and Lavoie [6] has used this to study the effects of initial conditions. To account for acceleration of flow through the contraction, they [4, 6] have converted streamwise distance to a decay time using

$$tU_0 = \int_0^x [\bar{U}(x)/U_0]^{-1} dx, \quad (1)$$

which simplifies to $tU_0 = x$ if $\bar{U} = U_0$. The mean velocity $\bar{U}(x)$ is the centreline velocity $U_{c1}(x)$ of the wind-tunnel flow in the

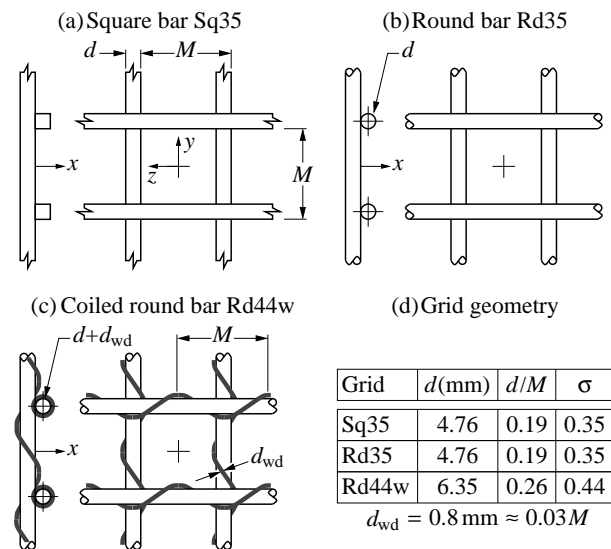


Figure 1: The biplanar grid; mesh solidity is $\sigma = d/M(2-d/M)$. The x coordinate axis lies on the centreline of the test section.

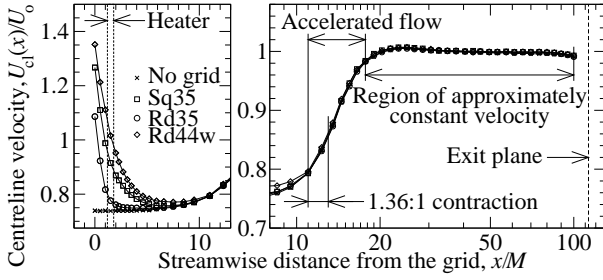


Figure 2: Centreline distribution of wind-tunnel velocity.

absence of a grid. Figure 2 shows measurements of $\bar{U}(x)$ with a Pitot-static probe and a (100-Pa) micro-manometer. The variation in wall pressure over the region of constant velocity ($18 \lesssim x/M \lesssim 100$) is no more than 1% of the dynamic pressure.

The flow is heated with a “mandoline” or grid of 0.5-mm-diameter Chromel-A wire located at $x = 1.5M$ downstream of the turbulence-generating grid [3, 12, 13]. The horizontal and vertical wires in the heater grid are separated by a gap of about $0.6M$ and have the same pitch as the turbulence-generating grid. Temperature is controlled by adjusting a variable-voltage (0 to 275 V) power supply.

Measurement technique

The temperature fluctuations are measured with a “cold-wire”. The wire ($d \approx 0.64 \mu\text{m}$; $l/d \approx 230$) is etched from a fine Wolston (Pt-10%Rh) and is operated with a locally manufactured (1-mA) constant-current anemometer. To obtain a sufficiently passive scalar, the heated flow is slightly warmer than the ambient air ($\Delta T \approx 2^\circ\text{C}$). The temperature coefficient of resistance of the wire, calibrated using a type-T thermocouple, is about $0.15 \Omega/^\circ\text{C}$.

The signals from the cold-wire probe are digitised with a $\pm 10.0\text{-V}$, 12-bit A/D converter. To minimise electronic noise, the signals are filtered and checked by plotting the temperature spectra. For the thermal fluctuation (θ , $^\circ\text{C}$) reported in

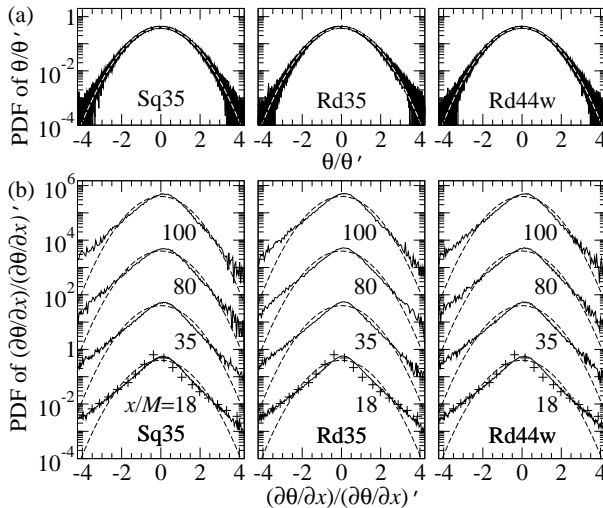


Figure 3: Probability density function; (a) θ/θ' ; $x/M \approx 18 \rightarrow 100$; (b) $(\partial\theta/\partial x)/(\partial\theta/\partial x)'$ — the top 3 set of curves are vertically offset by 2, 4 and 6 decades. The derivative uses the 3-point centre difference scheme. The normal distribution is shown as dashed lines. For the data of Tong and Warhaft [10] (+; a square-bar grid of 34% solidity; $x/M \approx 40 \rightarrow 200$; $Re_M = 9,700$; $Re_\lambda \sim 38$), the grid flow is not stretched by a contraction.

the following pages, each “data point” in the graphs is an average from (up to) 4 separate data records. The cut-off frequency of the low-pass filter is half the sampling rate and in each record, data is sampled for 30 seconds. To check that the data records are of sufficient duration, the probability density functions are compared with the normal distribution. In Figure 3, the signal fluctuation (θ) and its derivative ($\partial\theta/\partial x$) are non-dimensionalised using the respective standard deviations. The streamwise derivative is obtained by assuming the Taylor hypothesis ($\partial x = U_0 \partial t$). Figure 3 shows that the distribution for θ/θ' is approximately Gaussian (for up to 3.5 standard deviations from the mean), which suggests that the present sample size ($\sim 10^5$) is adequate for r.m.s. statistics. The probability density of $\partial\theta/\partial x$ is not Gaussian (Figure 3).

Results and discussion

For decaying homogeneous isotropic turbulence, Antonia et al. [2] show that a solution to the scalar transport equation takes the form of a power law,

$$\ln\{\theta^2/\Delta T^2\} = n \cdot \ln\{(t-t_0)U_0/M\} + \ln\{\alpha\}, \quad (2)$$

where t_0 , α and n are determined by the boundary conditions. Equation 2 applies to measurements which are downstream of the regions of initially developing turbulence and accelerated decay in the contraction [7, 11]. Figure 4 shows temperature variance in the range $22 \lesssim tU_0/M \lesssim 110$, where the time-averaged velocity is independent of streamwise distance ($U_{c1}/U_0 \approx 1 \pm 0.01$). To avoid possible effects of the duct exit, measurements stop about one duct width ($\sim 12M$) short of the duct exit plane.

The analysis begins by selecting a virtual origin which makes the decay exponent independent of streamwise distance from the grid. The method of curve fitting data points in Figure 4 is similar to the least-square technique of Mohamed and LaRue [9] and Lavoie [6]. For each grid, there are 27 data points spaced at intervals which appear uniform when plotted on a logarithmic scale (Figure 4).

In Figure 5, the decay exponent n is plotted as a function of “ x_1 ” — the first data point used for curve fitting. Figure 5 shows that the value of n depends on the virtual origin. The virtual origin $t_0 U_0/M$ is selected so that the decay exponent is independent of the range of the data used for curve fitting. This means that all of the data can be used for the curve fitting. Figure 6 shows typical behaviour of the curve fitting as virtual origin and curve-fitting range are varied. At optimum $t_0 U_0/M$, the fitting error is about 0.1%. If the virtual origin is placed at the grid, the error is no more than 1%. Table 1 is a summary of the curve-fitting results. The width of the 95% confidence interval for n is 0.02.

Inspection of the curve fits in Table 1 and a review of previous measurements in Table 2(a) show that, for a fixed power-law decay range with virtual origin at the grid, the round bar “Rd35” produces the largest scalar decay rate and the round bar “Rd44w” produces the smallest scalar decay rate. The velocity decay rate in *stretched* grid turbulence follows the same trend ($|m|, |n|$: Rd44w < Sq35 < Rd35). Lavoie [6] (page 119) observes that: “the anisotropy of the flow tends to increase the magnitude of m , since Rd44w generates the most isotropic turbulence ($u^2/w^2 \approx 0.99$).” Kármán and Howarth [5] show that, if turbulence is isotropic and self preserving, the decay is theoretically proportional to $(tU_0/M)^{-1}$. Since Lavoie [6] obtains powers of $m < -1$, this suggests that the grid turbulence is not isotropic. Rather, m depends on initial conditions but less so if the anisotropy (at the large scales) is reduced by the contraction [6]. For grid Sq35, the contraction tends to increase the displacement of the virtual origin and reduces $|n|$ by about 0.28 or 19% (see Tables 1 and 2(b)). Without a contraction, Zhou et al.

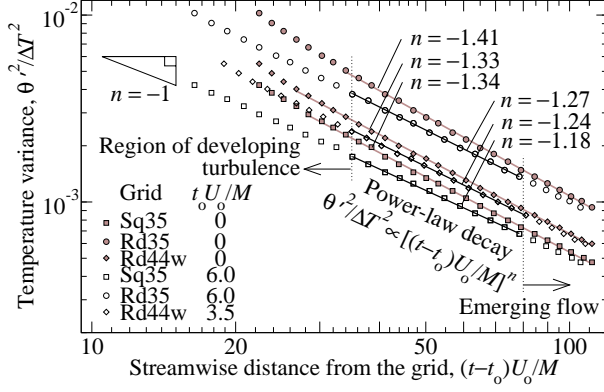


Figure 4: Decay of passive scalar downstream of each grid.

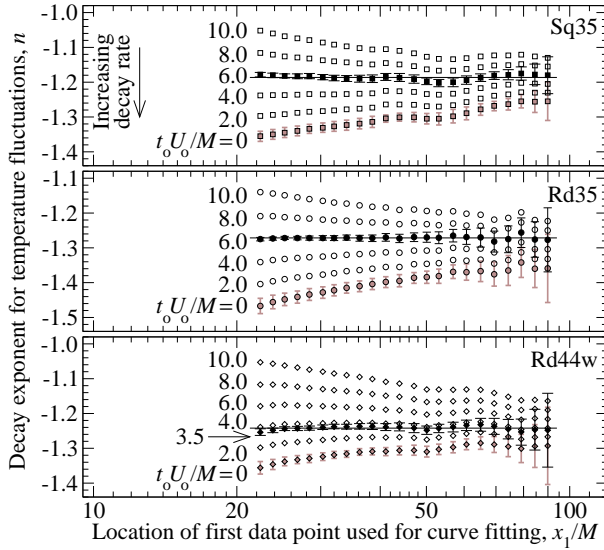


Figure 5: Power-law exponent (n) as a function of length of curve-fitting region [$x_1 \rightarrow x_{1\text{last}}$] and virtual origin; error bars are 95% confidence limits.

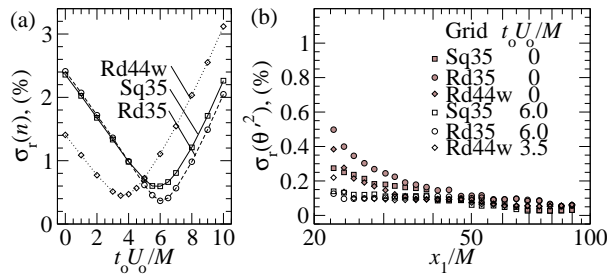


Figure 6: (a) Root-mean-square (r.m.s.) variation in n with changing virtual origin for the curve-fitting range [$x_1 \rightarrow x_{1\text{last}}$]; (b) r.m.s. curve-fitting error as a function [$x_1 \rightarrow x_{1\text{last}}$].

[12, 13] observe that the virtual origin for Sq35 grid turbulence is small (i.e. $t_0 U_0/M=1.5$) and so they do not adjust their data for virtual origin when calculating n .

For homogeneous isotropic turbulence (HIT), we assume the skewness ($S_\theta = \overline{\theta^3}/\theta'^3$) and kurtosis ($K_\theta = (\overline{\theta^4}/\theta'^4) - 3$) are very near zero (or close to Gaussian). However, grid turbulence only approximates HIT, and so its departure from ‘‘Gaussian’’ higher-order moments serves as a measure of the anisotropy.

Table 1: Summary of power-law curve fit. At 95% confidence, the uncertainty in n is ± 0.01 ; σ_r is the r.m.s. difference between the ‘‘log’’ of the data and Equation 2. The range of curve fit data is shown as $(t-t_0)U_0/M$.

Grid	$t_0 U_0/M$	$(t-t_0)U_0/M$	n	α	σ_r (%)
Sq35	0	28 to 110	-1.34	0.254	0.17
		35 to 80	-1.34	0.259	0.15
	6.0	16 to 110	-1.18	0.116	0.14
Rd35	0	34 to 110	-1.41	0.728	0.19
		35 to 80	-1.44	0.798	0.15
	6.0	16 to 110	-1.28	0.356	0.13
Rd44w	0	27 to 110	-1.33	0.315	0.19
		35 to 80	-1.32	0.299	0.10
	3.5	19 to 110	-1.25	0.209	0.22
		35 to 80	-1.24	0.193	0.10

Table 2: Review of decay exponents of velocity (m) and temperature (n) from the same wind tunnel (a) with a 1.36:1 contraction and (b) with no contraction. The anisotropy ratio is u'^2/v'^2 or u'^2/w'^2 . $Re_M = 10,400$, $Re_\lambda \sim 25 \rightarrow 55$. $\Delta T \approx 2^\circ\text{C}$. $t_0 U_0/M \approx 0$.

Group/Ref.	Grid	u'^2/v'^2	u'^2/w'^2	$(t-t_0)U_0/M$	$m(q^2)$	$n(\theta^2)$	
(a) Benaissa et al. [3]	Sq35	No data		25 to 77	No	-1.35*	
	Rd35				data	-1.42*	
	Rd44w					-1.24*	
	Lavoie [6]		No	0.99		-1.10	No
		Rd35	data [⊕]	1.07	30 to 77	-1.22	data
Sq35			1.11	34 to 77	-1.20		
(b) Lavoie [6]	Rd44w	No	1.30	29 to 80	-1.18	No	
	Rd35	data [⊕]	1.27	32 to 80	-1.19	data	
	Sq35		1.45	30 to 80	-1.04		
	Zhou et al. [13]		1.22	1.18		-1.33	-1.36
	[12]		1.19	1.16		-1.3	-1.4
				20 to 80		-1.46	

* In their Figure 3, Benaissa et al. [4] quote -1.11 (Sq35), -1.23 (Rd35) and -1.05 (Rd44w), but the tabulated values above seem to fit their data better.

⊕ Lavoie [7] assumes $v=w$ for calculating q .

Figures 7 and 8 show the higher-order moments of temperature and temperature gradient. The skewness and kurtosis of temperature are closer to zero for the square grid (Sq35) than for the round grids (Rd35 and Rd44w). Grid Rd35 gives the largest skewness and kurtosis. This suggests that the large-scale anisotropy from the square bars is weaker than from the round bars. Figure 7 shows a clear dependence of large-scale motion on the different grids. Since the three grids produce nearly identical trends in $S_{\partial\theta/\partial x}$ and in $K_{\partial\theta/\partial x}$ (Figure 8), we conclude that the small-scale motion has a weak dependence on the geometry of the grids.

A comparison of the skewness in Figure 7 with that of Mills et al. [8] shows the combined effect of the contraction, the wire wrapping of the round bars and a lower heating temperature (reducing $\Delta T \approx 5^\circ\text{C}$ to 2°C) is a more constant skewness

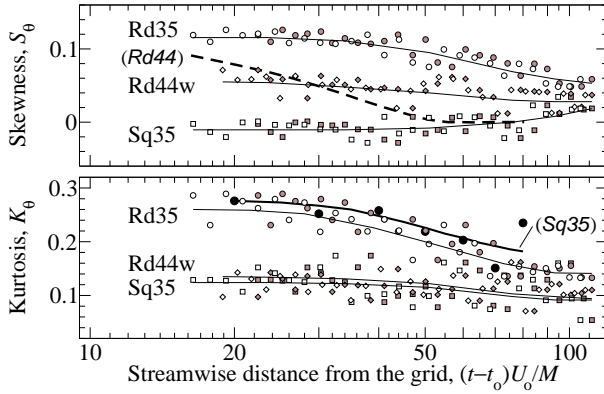


Figure 7: The skewness and kurtosis (the symbols are defined in Figure 4). For the data of Mills et al. [8] (—, a round-bar grid of 44% solidity (Rd44); $x/M \approx 15 \rightarrow 80$; $Re_M \approx 7,000$; $Re_\lambda \sim 19 \rightarrow 26$; $\Delta T \approx 5^\circ\text{C}$) and the unpublished Sq35 data (●) of Antonia, the grid flow is not stretched by a contraction.

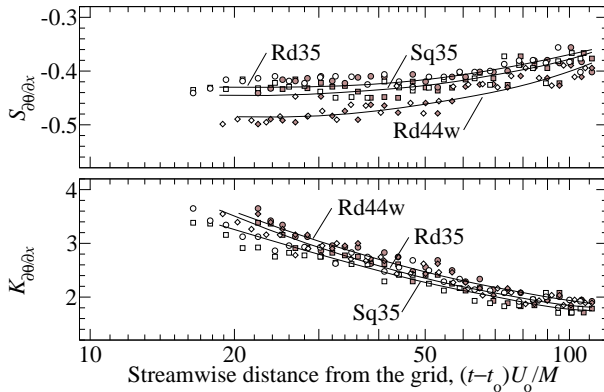


Figure 8: The skewness and kurtosis of temperature derivative (the symbols are defined in Figure 4). The curves are a visual guide only.

(Rd44w: $S_\theta \sim 0.05$). Unpublished data of Antonia shows that the unstretched Sq35 grid flow has a higher value of kurtosis ($K_\theta \sim 0.23$).

Antonia et al. [1] report that, for an unstretched grid flow, the moments of temperature derivative fall in the ranges $-0.34 \lesssim S_{\partial\theta\partial x} \lesssim 0.05$ and $2 \lesssim K_{\partial\theta\partial x} \lesssim 7$. Their measurements ($x/M \approx 29 \rightarrow 115$; $Re_M \approx 20,200$; $Re_\lambda \sim 40$; $\Delta T \approx 5^\circ\text{C}$) are obtained with a grid of round bars at 36% solidity which closely matches the present grid Rd35. Comparison of Antonia's et al. [1] data with the results in Figure 8 suggests that the contraction keeps the skewness small ($|S_{\partial\theta\partial x}| \lesssim 0.5$) and reduces the kurtosis ($K_{\partial\theta\partial x}$) by a factor of about 2.

Conclusions

This paper describes the effect of stretching on decaying passive scalar fluctuations in grid turbulence. Stretching of the flow is provided by a 1.36:1 contraction. Measurements with three different turbulence generating grids show that scalar fluctuations follow a power-law decay, and that the power-law exponent (n) depends on grid shape. The power-law decay exponent also depends on the virtual origin of the grid turbulence. The virtual origin is chosen so that the power-law decay formulae remain valid over the full range of the experimental data. Measurements of n are in the range -1.28 to -1.18 . However, in

isotropic turbulence, the theoretical decay exponent is -1 . For the square grid (Sq35), the effect of stretching increases the decay exponent from -1.46 to -1.18 .

Both decay rate exponent and skewness indicate that the grid with square bars produces less anisotropic turbulence than the grids with round bars ("Rd35 and Rd44w").

Acknowledgement

The ARC is gratefully acknowledged for its financial support.

References

- [1] Antonia, R. A., Chambers, A. J., Van Atta, C. W., Friehe, C. A. and Helland, K. N., Skewness of temperature derivative in a heated grid flow, *Physics of Fluids*, **21**, 1978, 509–510.
- [2] Antonia, R. A., Smalley, R. J., Zhou, T., Anselmet, F. and Danaïla, L., Similarity solution of temperature structure functions in decaying homogeneous isotropic turbulence, *Physical Review E*, **69**, 2004, 016305–1–11.
- [3] Benaïssa, A., Djenidi, L., Antonia, R. A. and Parker, R., Effect of initial conditions on the scalar decay in grid turbulence at low Re_λ , *Proceedings of the 16th Australasian Fluid Mechanics Conference*, 2007, 914–918.
- [4] Comte-Bellot, G. and Corrsin, S., The use of a contraction to improve the isotropy of grid-generated turbulence, *Journal of Fluid Mechanics*, **25**, 1966, 657–682.
- [5] de Kármán, T. and Howarth, L., On the statistical theory of isotropic turbulence, *Proceedings of the Royal Society of London. Series A.*, **164**, 1938, 192–215.
- [6] Lavoie, P., *Effects of initial conditions on decaying grid turbulence*, Ph.D. Thesis, The University of Newcastle, School of Engineering, Newcastle, Australia, 2006.
- [7] Mills, R. R. and Corrsin, S., Effect of contraction on turbulence and temperature fluctuations generated by a warm grid, *National Aeronautics and Space Administration; Memorandum*, **5-5-59W**, 1959, 58 pages.
- [8] Mills, R. R., Kistler, A. L., O'Brien, V. and Corrsin, S., Turbulence and temperature fluctuations behind a heated grid, *National Advisory Committee for Aeronautics; Technical Note*, **TN4288**, 1958, 67 pages.
- [9] Mohamed, M. S. and LaRue, J. C., The decay power law in grid-generated turbulence, *Journal of Fluid Mechanics*, **219**, 1990, 195–214.
- [10] Tong, C. and Warhaft, Z., On passive scalar derivative statistics in grid turbulence, *Physics of Fluids*, **6**, 1994, 2165–2176.
- [11] Warhaft, Z., An experimental study of the effect of uniform strain on thermal fluctuations in grid-generated turbulence, *Journal of Fluid Mechanics*, **99**, 1980, 545–573.
- [12] Zhou, T., Antonia, R. A. and Chua, L. P., Performance of a probe for measuring turbulent energy and temperature dissipation rates, *Experiments in Fluids*, **33**, 2002, 334–345.
- [13] Zhou, T., Antonia, R. A., Danaïla, L. and Anselmet, F., Transport equations for the mean energy and temperature dissipation rates in grid turbulence, *Experiments in Fluids*, **28**, 2000, 143–151.